Catal Lett (2017) 147:2116–2126
DOI 10.1007/s10562-017-2103-8

Al-Rich Ordered Mesoporous Silica SBA-15 Materials: Synthesis, Surface Characterization and Acid Properties

Zoulikha Talha[1] · Cherifa Bachir[1,2] · Sarah Ziri[3] · Salima Bellahouel[3] · Abdelkader Bengueddach[1] · Frédéric Villièras[4] · Manuel Pelletier[4] · Peter G. Weidler[5] · Rachida Hamacha[1]

Received: 9 February 2017 / Accepted: 6 June 2017 / Published online: 13 June 2017

Abstract Al–SBA-15 is an interesting mesoporous material having highly ordered nanopores and a large surface area, which is widely employed as catalysts and adsorbents, but relatively few studies on the surfaces properties of this type of materials have been carried out. The purpose of the present work was to advance knowledge on the textural properties of Al–SBA-15 by applying the accurate NLDFT method as well as to gain insight into the surface characterisation and acidic trend of this material. Mesoporous Al–SBA-15 molecular sieves, in three SiO_2/Al_2O_3 ratios: 50, 75 and 100 were accomplished by post-synthesis alumination in aqueous solution of a purely siliceous SBA-15 material. The obtained solids were characterized using powder X-ray diffraction (XRD), X-ray fluorescence (XRF), N_2 adsorption–desorption (BET/DFT), transmission electron microscopy (TEM), water adsorption and zeta potential measurements. The results indicate that Al atoms have been successfully incorporated into the framework of the hexagonal mesoporous SBA-15. The aluminum introduced amount has remarkably affected the surface properties of the SBA-15 solid, indeed microporosity decreased. Furthermore, the esterification test showed that the Al–SBA-15 material exhibit Brønsted acid properties with an interesting activity leading to yields of ~90% of biodiesel.

✉ Rachida Hamacha
rachidahamacha@gmail.com

[1] Laboratoire de Chimie des Matériaux L.C.M., Université d'Oran 1 Ahmed Ben Bella, BP-1524 El-Mnaouer, 31000 Oran, Algeria

[2] Laboratoire de Chimie Appliquée LAC, C.U. Aïn-Témouchent, Route Sidi Bel Abbes BP-284, 46000 Ain Temouchent, Algeria

[3] Laboratoire de Synthèse Organique Appliquée, Université d'Oran 1 Ahmed Ben Bella, BP-1524 El-Mnaouer, 31000 Oran, Algeria

[4] Laboratoire Interdisciplinaire des Environnements Continentaux, UMR 7360 CNRS - Université de Lorraine, 15 Avenue du Charmois, 54500 Vandoeuvre-les-nancy, France

[5] Institute of Functional Interfaces, Karlsruher Institut fu¨r Technologie KIT, Hermann-von-Helmholtz-Platz 1, 76344 Eggenstein-Leopoldshafen, Germany

Graphical Abstract

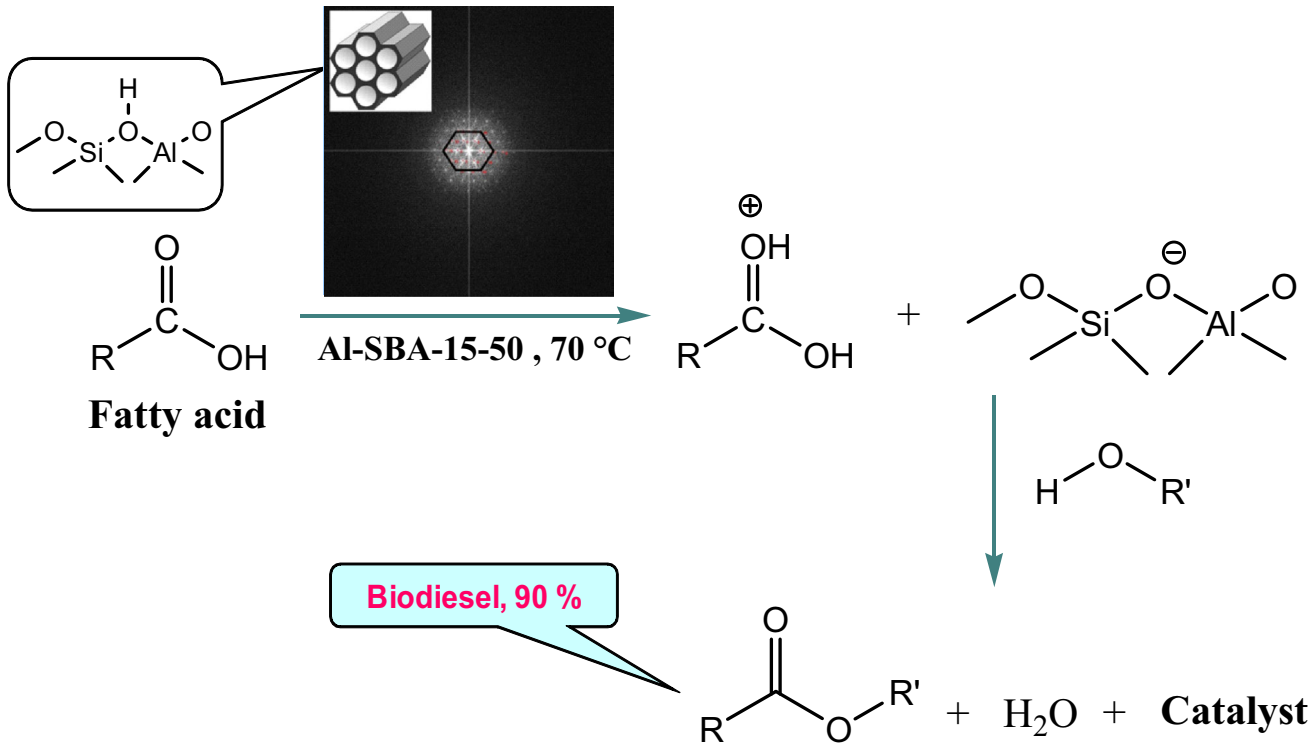

Keywords Al–SBA-15 · Post-synthesis · Zeta potential · Water adsorption · Brønsted acid

1 Introduction

Mesoporous silica, with hexagonal array and uniform mesoporous channel are materials exhibiting pore of diameters in the range of 2–50 nm [1]. Since the mesoporous siliceous materials were synthesized, there has been an increasing interest in the tailoring of these materials for potential applications in separation/adsorption processes, and catalysis when applied in heterogeneous reactions involving large organic molecules for wide applications than that of microporous solids such as zeolites [2]. In 1998, a prominent research which produces hexagonal array of pores namely as Santa Barbara Amorphous no 15 (SBA-15), with larger pore size (4.6–30 nm), thicker pore walls (3.1–6.4 nm) and higher surface area (up to 1000 m^2/g), was a research challenge in mesoporous material development [3]. SBA-15 also shows greater thermal, mechanical and chemical resistance properties that make it a preferable choice than other types of catalysts [4] and than the conventional MCM-41 support. This material is prepared under acidic conditions and exhibits better hydrothermal and thermal stabilities [3, 5]. Despite promising properties of pure siliceous SBA-15 in catalysis, there is still a need to modify or functionalize SBA-15 in order to overcome its limitation of low acidity strength [6]. Incorporation of heteroatoms such as aluminium into the highly structured SBA-15 materials [7, 8] enhance and optimize its catalytic activity. Up to now, there are two typical approaches to synthesize conventional mesoporous aluminosilicates: direct synthesis [9, 10] and post-synthesis [11, 12]. Ma et al. [13] discovered that, in comparison with direct synthesis method, the acidity and catalytic activity of Al–SBA-15 synthesized by post-grafting method has shown to be higher due to formation of Lewis and Brønsted acid sites. In another application [14], the activity of Al–SBA-15 was proved to be affected by hydrolysis ratio and aluminium concentration which could be correlated to various ratio of Si/Al. Hu et al. [15] found that the Brønsted acid sites in dehydrated mesoporous Al–SBA-15 materials are not in the form of bridging hydroxyl groups, but originate from terminal silanol groups in the vicinity of aluminium atoms and no Lewis acid sites can be found in Al–SBA-15 samples.

Beside determination of structural and textural properties, surface functionality strongly affects the efficiency of materials. The hydrophobic nature of porous materials have been studied by a number of investigators [16–22]. The structural silanol defects (Si–OH) consist of terminating silanol groups of the Si–O–Si network wherein oxygen atoms no longer bond to silicon atoms and also from the

internal silanol groups where the Si–O–Si bonds are broken. The hydrophobic nature of the material has also been studied by the adsorption of water molecules on material under controlled vapor pressures using thermogravimetry [16], manometric sorption [17, 18] and Diffuse Reflectance Infrared Fourier Transform (DRIFT) [18]. Inagaki et al. [17] reported the large hysteresis in adsorption isotherms of water on FSM-16 and the hydrophobicity of FSM-16, which was changed by treatment with water vapor. Pires et al. [18] discussed and related the information on the hydrophobicity degree obtained from both water adsorption isotherms and from Diffuse Reflectance Infrared Fourier Transform (DRIFT) for a set of porous materials: MCM-41, SBA-15, two xerogels and also different porous clays heterostructures. However, to access the hydrophilic–hydrophobic properties of the materials and to relate these properties with the structure and the surface chemistry, in a way that different materials can be compared, the water adsorption, in particular through the analysis of the A_{max} parameter, should be preferred. This adsorption potential theory was used to fit the water adsorption isotherms on all MFI type zeolite adsorbents as studied by Zhang et al. [19], and hierarchical zeolites by Thommes et al. [20]. A strong correlation is known to exist between water uptake and the content of framework aluminium [21], in MFI zeolites and the differences in adsorption observed between different Si/Al ratios are consistent with the increased hydrophilicity expected based on the greater aluminium content in the former. Zhao et al. [22] investigated the adsorption isotherms of water adsorption on the MFS (fluorine-containing mesoporous silica) and suggested the weak interaction between the water vapor and the MFS surface. Material characterization results showed that MFS has stronger hydrophobicity than SBA-15 and MCM-41 due to the presence of fluorine-containing group.

The zeta potential (ζ) has been extensively studied in recent years [23–26] for the determination of the isoelectric point of solids. The ζ value measured for pure siliceous SBA-15 is positive only at pH value below 3.5. The measure of zeta potential is very important for the application of SBA-15 materials on aqueous solutions.

Thus, the investigation of the surface charge and the surface hydrophobicity of Al–SBA-15 have to be considered for a better characterization of synthesized solids.

Esterification of carboxylic acids with alcohols represents a well-known and important category of liquid-phase reactions of considerable industrial interest due to the enormous practical importance of organic ester products [27–29].

Currently, the acid-catalyzed esterification of long-alkyl chain fatty acids (FA) has spurred a great deal of interest, because long-chain FA alkyl esters can be used as a biofuel. One of the main products obtained by esterification of long chain fatty acids is biodiesel, whose use has several environmental benefits [30]. Esterification is usually carried out in the homogeneous phase in the presence of acid catalysts such as sulfuric and *p*-toluene sulfonic acids [31]. However, the use of homogeneous catalysts poses several problems, such as difficulty in separation and recovery and environmental pollution [32].Hence the use of recoverable catalyst remains the best solution. Thus catalysts as Al–MCM-41, Al–SBA-15 [33–38] were proposed and achieved high catalytic activity in the biodiesel synthesis reactions.

The aim of the present work, is to perform the post-synthesis of Al–SBA-15 with various aluminium concentrations ($SiO_2/Al_2O_3 = 50$, 75, and 100) and to characterize scrupulously the obtained aluminium post grafted SBA-15. One of the characterization methods involves the study of the surface charge (zeta potential measurements) as well as the study of surface hydrophobicity via water vapour adsorption. The acidity of these supports will be tested in the biodiesel production via esterification of lauric, palmitic and stearic acid with methanol and ethanol. Another important fact of this work is the application of the DFT method rather than the BJH in the pore analysis.

A combination of interesting structural/textural data of Al–SBA-15 materials with their acidity will be studied. In particular, an attempt will be made to establish correlation between surface charge/hydrophobicity and catalytic activity in the esterification of fatty acids.

2 Experimental Section

2.1 Materials

The purely siliceous SBA-15 mesoporous material, denoted as Si–SBA-15, was prepared according the procedure described by Zhao et al. [3, 39]. 2 g of Pluronic P123, used as structure-directing agent ($EO_{20}PO_{70}EO_{20}$, average molecular weight 5800, Aldrich), was dissolved in 15 g of deionized water and 60 g of 2 M HCl solution under stirring at 40 °C. Then 4.25 g of tetraethyl orthosilicate (TEOS 98 wt%, Aldrich) was added into that solution with stirring at 40 °C for 2 h. The mixture was crystallized at 100 °C for 2 days in a Teflon lined autoclave. The product was filtered, washed, dried at 100 °C overnight and then calcined in air from room temperature up to 550 °C for 6 h to remove the organic templates.

The incorporation of Al into SBA-15 mesostructure was carried out by post-synthesis method using sodium aluminate as Al source (Al_2O_3 50–60%, Na_2O 40–45%, Sigma-Aldrich) [40]. In a typical procedure, various amounts of sodium aluminate, corresponding to different SiO_2/Al_2O_3 ratios ($SiO_2/Al_2O_3 = 50$, 75, 100), were dissolved in 50 g of deionized water. This procedure is followed by stirring

for 10 min and then an appropriate amount of calcined Si–SBA-15 was added to the above mixture. This mixture was stirred at room temperature for 20 h and then filtered, washed, air-dried and finally calcined at 550 °C for 5 h. The prepared samples were designated as Al–SBA-15-SiO_2/Al_2O_3 molar ratio. For the catalysis tests, catalyst ionic exchange was carried out in an excess of 0.5 M NH_4NO_3 solution at 80 °C for 2 h. Next, the catalysts were calcined in an oven at 450 °C for 4 h, giving the protonated solid H–Al–SBA-15.

2.2 Characterization Methods

X-ray diffraction (XRD) was carried out on a Bruker AXS D8 advance diffractometer working with CuKα radiation (λ = 1.54056 Å) equipped with a Lynxeye Trade Mark (TM) position sensitive stripe detector. Diffractograms were recorded over the range 0.6–6 °2θ (step size 0.02 °2θ, step time 4 s).

Nitrogen adsorption adsorption–desorption measurements were performed at 77 K using a Quantachrome Autosorb-1MP instrument in the relative pressure range p/p0 from 10^{-5} to 1. The samples were outgassed overnight at 300 °C prior to the adsorption analysis. Specific surface areas SSA were calculated according to the Brunauer–Emmett–Teller (BET) equation [41]. The nonlocal density functional theory (NLDFT) is explored based on the normal DFT method. NLDFT is able to correlate the properties of gas molecules with their adsorption performance in different pore size. The NLDFT model is accurate in depicting the fluid approaching the pore walls [42] and getting more reliable size estimation, thus, the NLDFT has been applied in this work. For the SBA-15 samples, the NLDFT was used to calculate the mesopore volume (V_{mes}, pore width between 2 and 50 nm), average pore diameter (D_{pDFT}) and wall thickness (bp_{DFT}) from the adsorption branch assuming cylindrical pore geometry. The NLDFT cumulative pore volume and the corresponding differential pore volume distribution curves of all materials were also illustrated. The N_2 adsorption–desorption isotherms of samples have been also established, in order to get information on the forms of the isotherms and their hysteresis loop which are related to the pore nature existing in their structure [43, 44]. The chemical composition were analysed by X-ray fluorescence (XRF) (Philips PW2400). The structure and morphology of the mesoporous materials were examined by analytical transmission electron microscopy (TEM) using a Philips CM20.

For zeta potential measurements, electrokinetic analysis were obtained by electrophoresis using a Zetaphoremeter IV from CAD Instrumentation Company. The particles were suspended in ultra pure water and the measurements of the zeta potential were obtained from electrophoretic mobility, according to the Smoluchowski equation, as a function of the pH [45]. The measurements were achieved in 0.1 M NaCl solution. The pH was controlled either by adding NaOH or HCl diluted solutions.

Water vapor adsorption–desorption isotherms were obtained in automatic device conceived and realized in LEM-GRESD (University of Nancy).This measurement was carried out using a lab-built quasi-equilibrium setup designed around a Setaram MTB 10^{-8} symmetrical microbalance. Water vapor was supplied to the sample (thermostated at 30 °C) from a source kept at 41 °C at a slow flow rate to ensure quasi-equilibrium conditions at all times. The simultaneous recording of mass uptake and equilibrium pressure directly yields the water vapor adsorption isotherm. The experimental conditions were a sample mass of 105 mg and an outgassing at 120 °C during 18 h under a residual pressure of 1 Pa.

2.3 Esterification Test

The acid catalytic activity of the prepared H–Al–SBA-15 was assessed in the esterification of fatty acid with alcohols. We used 5 wt% of the protonated catalyst with a mixture of alcohol (16 mL) and fatty acid (1 mmol) under stirring at 70 °C.

After the esterification test, the reaction mixture was filtered to recover the catalyst and separate the organic phase. The obtained organic product was washed and dried over magnesium sulphate $MgSO_4$. The melting points were taken using a banc Kofler. The analytical chromatographies (CCM) were carried out on an analytical silica plate.

Proton nuclear magnetic resonance (^{1}H-NMR) spectra were recorded at 300 MHz on a Brucker AC. The chemical shift δ is given in ppm and the coupling constant in hertz, TMS (tetramethylsilane) being taken as internal reference. The signal multiplicities are indicated as: s (singlet), d (doublet), t (triplet), q (quadruplet), m (multiplet).

Fourier transform infrared (FT-IR) spectra of samples in KBr pellets were recorded on a spectrometer with Fourier transform JASCO-4200.

3 Results and Discussion

3.1 Elemental Analysis and XRD Investigation

The SiO_2/Al_2O_3 molar ratios, before and after post synthesis alumination, are listed in Table 1. These results indicate that Al was incorporated into the SBA-15 framework by the procedure performed in this work. The Si/Al ratios of all Al–SBA-15 samples were lower than those in the initial synthesis mixture. Thus, the Al content of the products increased compared with the initial Al content. Kao et al.

Table 1 XRF and XRD data of Si–SBA-15 and Al–SBA-15 samples

Sample	SiO_2/Al_2O_3[a]	SiO_2/Al_2O_3[b]	$\Delta_{Si/Al}$[c]	d_{100}[d] (nm)	a_0[e] (nm)
Si–SBA-15	∞	–	–	9.71	11.17
Al–SBA-15–100	100	60.98	39.02	9.50	10.97
Al–SBA-15–75	75	48.00	27.00	9.71	11.17
Al–SBA-15–50	50	29.48	20.52	9.94	11.47

[a]Initial SiO_2/Al_2O_3 in the gel composition

[b]SiO_2/Al_2O_3 after post synthesis (by XRF)

[c]Difference in both SiO_2/Al_2O_3 ratios

[d]Basal spacing

[e]Unit cell parameter

[46] related this behaviour to a loss of silica via the alumination process. This loss of silica might have happened since the alumination was applied with pH value close to 9. It is notable that the Si/Al ratio of 50 (50-Al–SBA-15 sample), which is the highest framework aluminium content incorporated in Si–SBA-15, exhibit the low silica loss compared with the other ones.

The XRD patterns of the Si–SBA-15 and Al–SBA-15 with different Si/Al ratios ($SiO_2/Al_2O_3 = 50$, 75 and 100) are shown in Fig. 1.

These samples exhibit four distinct diffraction peaks that can be indexed as (100), (110), (200), and (210) reflections of the hexagonal symmetry revealing the high structural organization of the mesoporous structure in the P6mm space group similar to that observed in siliceous SBA-15 [5] and Al–SBA-15 [15]. Another additional weak peak at $2\theta = 2.6°$ corresponds to the (300) scattering reflection [5] indicating that all the prepared SBA-15 samples have a high degree of hexagonal mesoscopic organization.

The well resolved diffraction patterns reveal that all samples retain the characteristic of the hexagonal mesostructure even after Al-functionalization. Globally, the 100 peak shifted toward lower θ values (Table 1) with a slight increase of the d_{100} basal spacing and the lattice parameter a_0, calculated according to the formula $a_0 = 2d_{100}/\sqrt{3}$. These results can be explained by the Al clustering into the mesoporous framework of SBA-15. Such evolution can be easily explained by the much larger ionic radius of Al^{3+} (67.5 pm) when compared with the Si^{4+} ones (54 pm). Moreover, the intensity of the observed peaks for the Al–SBA-15 samples is weaker at lower Si/Al ratio, indicating that the ordered mesoporous structure is affected by the incorporated aluminium content. A similar result was reported by Chen et al. [47]. In another work, Li et al. [48] suggested that the decrease in the reflection peak intensity of the d_{100} indicated that the grafting happened inside the pore channels.

3.2 Textural Properties

The adsorption–desorption isotherms of the pure siliceous SBA-15 and Al–SBA-15 at various Si/Al ratios are displayed in Fig. 2.

The isotherm shapes of all samples correspond to type IV [43] characteristic of mesoporous materials. Three different regions can be seen on the isotherm plots: (i) a linear region due to monolayer-multilayer adsorption in mesopores; (ii) a steep region due to capillary condensation within these mesopores; (iii) a second linear region due to multilayer formation on the external surface of the grains.

The existence of mesoporosity is also supported by the presence of a clear type-H1 hysteresis loop with capillary condensation step occurring at higher relative pressure.

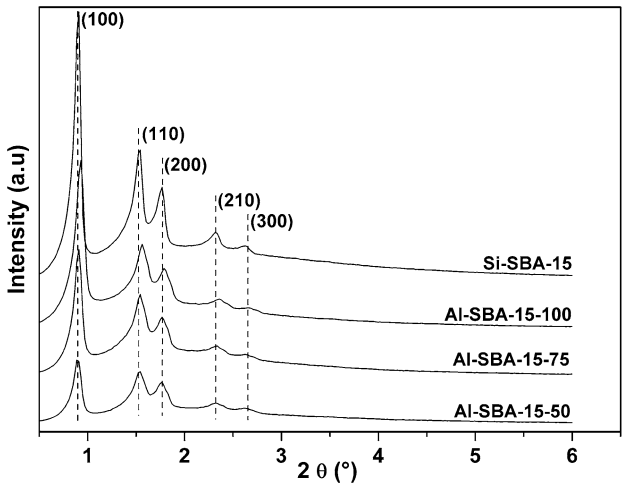

Fig. 1 XRD patterns of Si–SBA-15 and Al–SBA-15

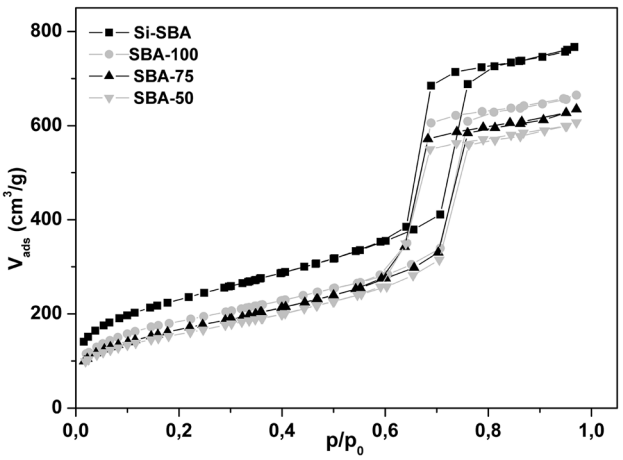

Fig. 2 N_2 isotherms of Si–SBA-15 and Al–SBA-15

Similar feature for purely siliceous SBA-15 was found by Zhao et al. [5].

These results suggest that the prepared samples exhibit highly ordered mesoporous structure even when a large amount of Al species is introduced.

Textural parameters including specific surface areas SSA, mesoporous volume V_{mes}, average pore diameter (D_{pDFT}) and wall thickness bp_{DFT} (a_0-D_{pDFT}) of the prepared materials are summarized in Table 2. The obtained results revealed that all samples showed higher surface areas and porosity. Furthermore, the SSAs and the pore volumes decreased with decreasing SiO_2/Al_2O_3 molar ratios. The reduction of these parameters might be due to an alkaline dissociation of the pore structure leading to the pore structure degradation. Similar studies on Al post synthesis of SBA-15 in basic media was reported by Kao et al. [46] and Kumaran et al. [49]. Moreover, the pore diameter slightly decreased as the aluminium content increased. It seems that this textural parameter has no direct relationship with the Al amount. However, an increase of the wall thickness is obtained (Table 2). This trend can be probably caused by the presence of the bond length of Al–O (183.6 pm) in the wall surface of Al-containing samples which is higher than Si–O (158 pm) as it has been mentioned in Al–MCM-41 materials [50]. This property is directly related to the thermal stability and catalytic activity of the Al–SBA-15 materials and is very beneficial for catalytic application.

Several studies have focalised on micropores present in the purely siliceous SBA-15 as indicated by t-plot analysis of the nitrogen isotherm [51–54] which showed that the total pore volume of SBA-15 contains 0–8% of micropores. Miyazawa et al. [51] studied the variation of microporosity in the walls of SBA-15 by varying the synthesis conditions. Galarneau et al. [52] prepared the SBA-15 with no micropores. They suggested that the micropores in the walls are replaced by mesopores because of high-temperature synthesis. Esparza et al. [53] discussed the variation of the micropores corresponding to the ~7–8% in the total pore volume which was confirmed by Sonwane et al. [54]. The structure consists of main mesopore channels and extra pores (which could be micropores and mesopores) in the pore wall. These authors concluded that the microporosity can be controlled via the synthesis conditions. The micropores volume calculated for our materials as a function of Si/Al ratio is given in Table 2. It can be seen that the micropores volume of aluminium incorporated SBA-15 decreases as the aluminium content increases, this could be attributed to the possible blocking of micropores by Al addition.

Table 2 Textural properties of Si–SBA-15 and Al–SBA-15 samples

Sample	SSA[a] (m^2/g)	V_t[b] (cm^3/g)	V^c_{micro} (cm^3/g)	D_{PDFT}[d] (nm)	b_{pDFT}[e] (nm)
Si–SBA-15	816	1.15	0.0350	7.6	3.57
Al–SBA-15–100	647	1.00	0.0088	7.6	3.37
Al–SBA-15–75	593	0.96	0.0000	7.3	3.87
Al–SBA-15–50	553	0.91	0.0030	7.3	4.17

[a]Specific surface area

[b]Total volume

[c]Micropores volume

[d]Pore diameter determined by DFT

[e]Wall thickness (a_0–D_{pDFT})

Figure 3 shows the NLDFT cumulative pore volume and the corresponding pore size distribution curves of SBA-15 and Al–SBA-15. For all the synthesised solids, the distribution presents a narrow pore size distribution centred around 7.5 nm (mesoporous range). The corresponding cumulative pore volume shows one step associated with the pore distribution maxima.

Both the N_2 adsorption and XRD results indicate that well defined hexagonal mesoporous structure are obtained at all Si/Al ratios of Al–SBA-15 and in the purely SBA-15.

3.3 Water Adsorption

Figure 4 shows adsorption–desorption isotherms of water vapour on SBA-15 samples. The adsorption isotherms are of type V, in the IUPAC classification, suggesting a weak interaction between water vapor and the hydrophobic surface of the SBA-15 surface [18]. A larger amount of adsorption and unclosed hysteresis for Si–SBA-15 isotherm suggests an irreversible adsorption of water. This feature has also been observed by Inagaki et al. for FSM-16, they correlated the large hysteresis of the water isotherms to the capillary condensation phenomena and the difference in contact angle between adsorption and desorption [17].

Moreover, the results indicate that the adsorbed amount of water decreases with decreasing Si/Al ratio. The change of surface properties is caused by the aluminium incorporation into the SBA-15 framework and is attributable to lower silanol units concentration after Al–SBA-15 post synthesis. This result is in good agreement with the already establishment better hydrothermal stability of aluminium incorporated mesoporous materials when compared to purely siliceous materials [55, 56].

Pires et al. [18] tried to quantify the hydrophobic character by evaluating the adsorption potential A which is defined as the work done by the adsorption forces in delivering the molecules from the gas phase to the sorbed phase on the adsorbent surface [57]. For one mole of ideal gas, the adsorption potential A can be estimated as: $A = RT \ln (P_0/P)$. This value was calculated at the point where the adsorption isotherm changes the curvature (convex to concave) in relation to the pressure axis. The obtained values

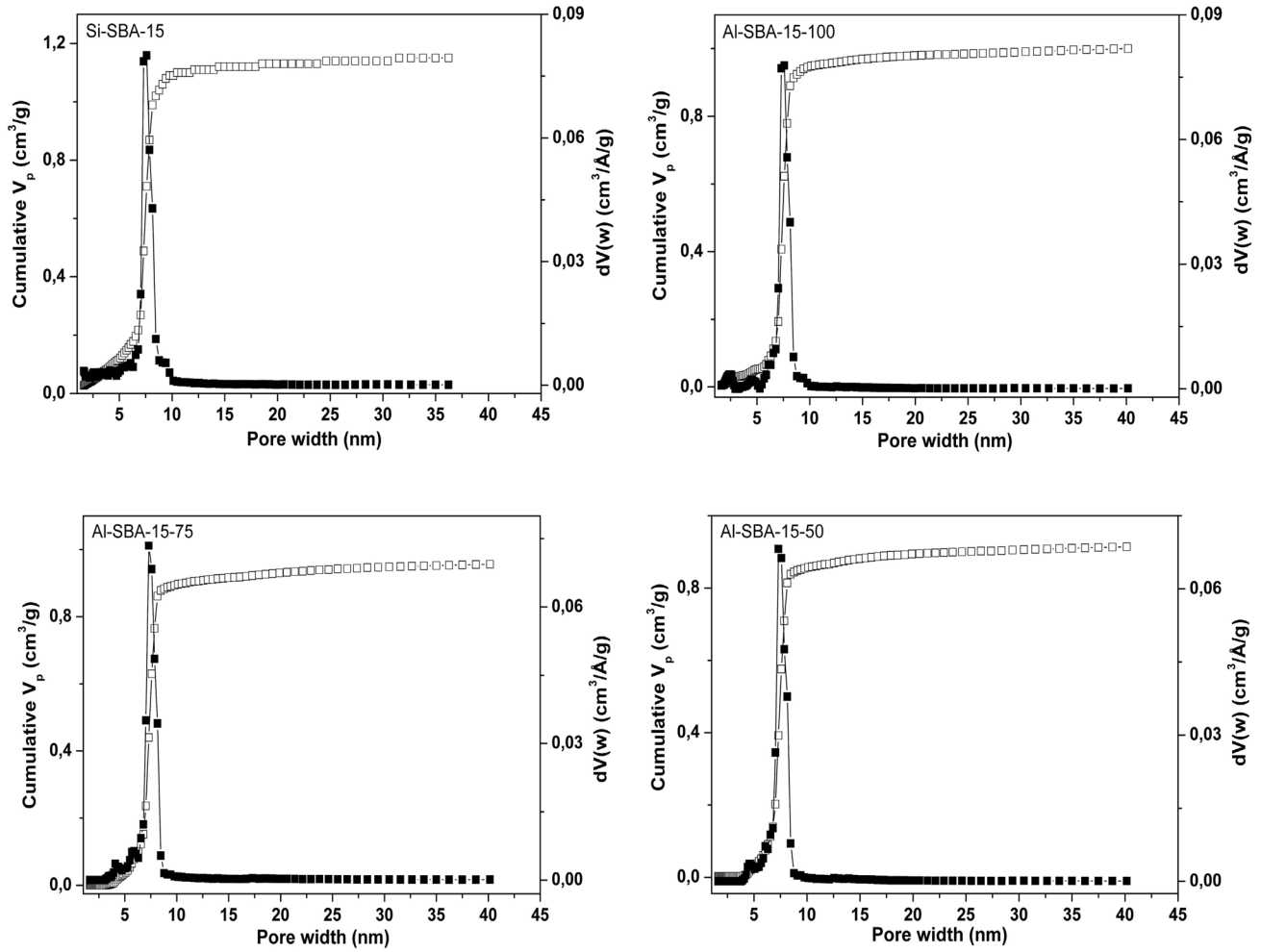

Fig. 3 NLDFT pore size distribution of Si–SBA-15 and Al–SBA-15. *Full symbols*/right y-axis: differential pore volume distribution curves, *open symbols*/left y-axis: cumulative pore volume curves

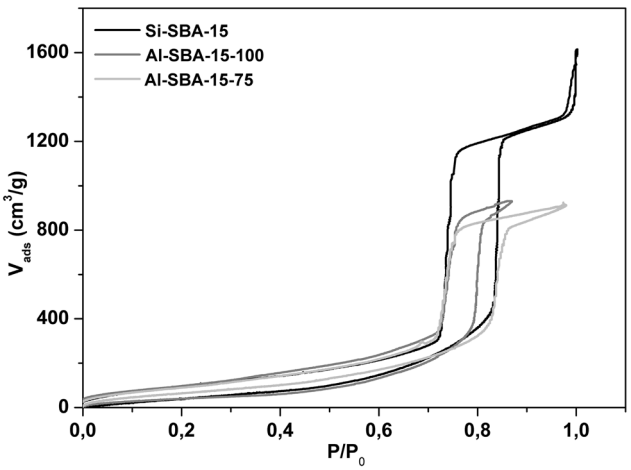

Fig. 4 Water isotherms of Si–SBA-15, Al–SBA-15–100 and Al–SBA-15–75

for the synthesized materials Si–SBA-15, Al–SBA-15–100 and Al–SBA-75 are respectively 0.45, 0.58 and 0.49 (kJ/mol). It can be seen that the purely siliceous SBA-15 has the lowest A corresponding to the most hydrophobic character.

3.4 Surface Charge Determination

Figure 5 shows the zeta potential ζ as a function of pH value for Si–SBA-15 and Al–SBA-15. The ζ potential of pure silica SBA-15 is negative only at pH value above 4, as surface silanol groups (Si–OH) tend to lose a proton and form (Si–O^-) species. Moreover, the sample exhibits a point of zero charge PZC at pH 3.2. A similar study reported by Song et al. [58] for pure siliceous SBA-15 indicate that the PZC was at pH 3.5.

However, in the case of Al–SBA-15, for all Al-modified samples, it can be observed that these materials have no point of zero charge and they exhibited negative zeta

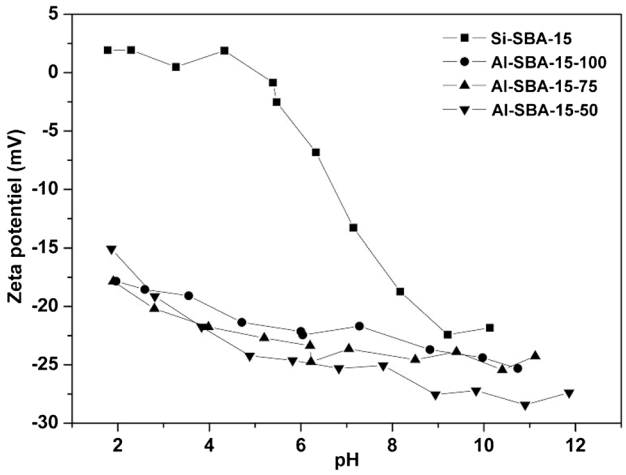

Fig. 5 Zeta potential curves of Si–SBA-15 and Al–SBA-15

potential in the studied pH range from 2 to 10. Thus, aluminum introduced amount has remarkably altered the surface charge of the solid due to the presence of AlO_4 tetrahedrons.

The change of surface charge confirms again the aluminium incorporation into the SBA-15 framework and is attributable to the decrease of the silanol units concentration after aluminium incorporation in SBA-15 solids. Such change in the surface charge creates a favourable substrate for the adsorption of cationic species.

3.5 Transmission Electron Microscopy (TEM) Analysis

TEM images of the pure siliceous SBA-15 and the Al–SBA-15 samples with other SiO_2/Al_2O_3 atomic ratios are presented in Fig. 6. The TEM image of Si–SBA-15 material clearly exhibit a well ordered regular arrangement of hexagonal array of atoms on the host Si–SBA-15 further confirming that it is a high quality mesoporous molecular sieve. After alumination, TEM measurement shows that Al–SBA-15 retains highly ordered mesostructure.

The distance between two consecutive centers of hexagonal pores estimated from the TEM image is ca. 11.35 nm of Si–SBA-15, 11.12 nm of Al–SBA-15-100, 11.45 nm of Al–SBA-15–75 and 11.46 nm of Al–SBA-15–50. The average thickness of the wall is ca. 3.78 nm of Si–SBA-15, 3.71 nm of Al–SBA-15–100, 4.16 nm of Al–SBA-15–75 and 4.17 nm of Al–SBA-15–50 and the pore diameter is around 7.57 nm of Si–SBA-15, 7.41 nm of Al–SBA-15–100, 7.29 nm of Al–SBA-15–75 and 7.29 nm of Al–SBA-15–50. These results are in agreement with the N_2 adsorption data (Table 2). Moreover, the electronic diffraction of Al–SBA-15–75 confirms its well defined unit cell of hexagonal pattern and the good organization of channels (Fig. 6c, inset).

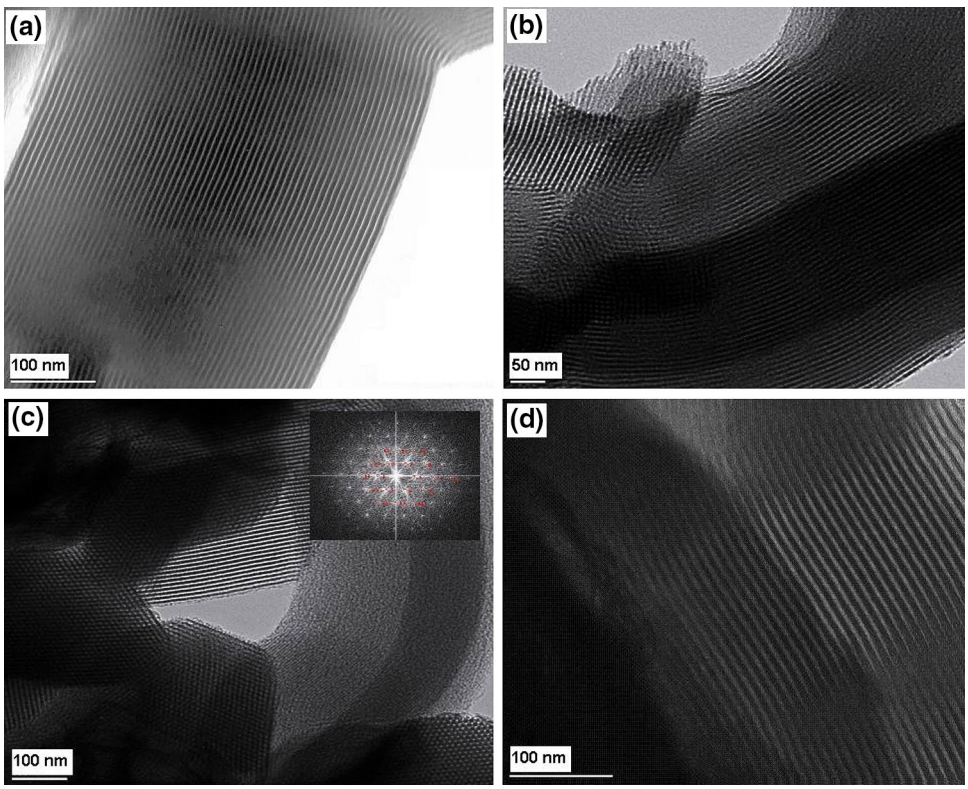

Fig. 6 TEM images of: **a** Si–SBA-15, **b** Al–SBA-15–100, **c** Al–SBA-15–75 with *inset* of electronic diffraction pattern, and **d** Al–SBA-15–50

Table 3 The effect of SiO_2/Al_2O_3 molar ratios and reaction time on the esterification of lauric acid and methanol over Al–SBA-15 catalysts

SiO_2/Al_2O_3 molar ratios effect		Reaction time effect (Al–SBA-15–50)	
Samples	Conversion (%)	Time (h)	Conversion (%)
Al–SBA-15–50	85	2	85
Al–SBA-15–75	79	8	90
Al–SBA-15–100	76	24	91

Reaction conditions: lauric acid (16 mL), methanol (1 mmol), Al–SBA-15 (5 wt%), 70 °C

3.6 Acid Properties

The esterification test was conducted with a mixture of lauric acid and methanol. In a preliminary study the reaction was carried out with different aluminium content by varying the Si/Al ratio of the activated Al–SBA-15 materials keeping the same mole ratio of acid to alcohol for 2 h at 70 °C. It is clearly seen (Table 3) that all Al incorporated SBA-15 samples are active. The highest conversion value is obtained with low Si/Al ratio corresponding to large concentrations of catalytic sites. This feature correlates directly with the high Brønsted acidity at higher Al content.

Since the number of acid sites decreases with an increase of the Si/Al ratio, the hydrophobic and hydrophilic properties of the catalyst are involved in the catalytic process. When the Si/Al ratio is decreased, i.e. the aluminium amount increases, the hydrophilicity will increase as well. Aluminum incorporation leads to the decrease in the Si–OH groups into the channel wall as well as the formation of additional surface hydroxyl Si(OH)Al groups with strong Brønsted acidity.

Moreover, the obtained results indicate that Al incorporation in the Si–SBA-15 leaves fewer free silanols and Lewis acid sites. Liang et al. [37] observed new signals, at 1546 and 1639 cm^{-1}, in the IR spectra of pyridine adsorbed on Al–SBA-15 catalysts. They suggested that Brønsted acid sites were generated in these samples which indicate that the acid strength of the Brønsted acid sites has been enhanced after Al-incorporation.

Since the higher charged Si^{4+} ion was replaced by the lower charged Al^{3+} ion in the silica framework, the net negative charge of Al–O–Si clearly differed from that of Si–O–Si. This trend is supported by the negative surface charge in the zeta potential measurements of the Al–SBA-15 catalysts and is one of the possible reasons for the increase in the Brønsted catalytic acidity.

Furthermore, the degree of conversion as a function of the reaction time for Si/Al = 50 is established (Table 3). The reaction yield increases slightly with increasing contact time up to 8 h. After 24 h, no significant increase was obtained.

The reaction conditions for further esterification test using H–Al–SBA-15 catalyst are: Si/Al ratio of 50 and reaction time 8 h.

For further reaction investigation, the catalytic activity was tested for the different acids (lauric acid, palmitic acid and stearic acid) with methanol as well as for lauric acid with two different alcohols (methanol and ethanol) under the previously reaction conditions (Table 4).

In both cases, it is noted that the reaction yield falling to lower values for longer chain length of fatty acid and alcohol. This trend is more accentuated with increasing the alcohol chain length. This result can be explained by the difference in steric and inductive effects of the used alcohol which is directly related to the positive charge of carbonium ion after nucleophic reaction with lauric acid as outlined in literature [33]. Since methanol can give a carbonium ion with higher degree of positive charge compared to that of ethanol, the esterification conversion with methanol becomes higher than that with ethanol.

Moreover, the decreasing trend in fatty acid reactivity with increasing alkyl chain length has to be considered. Steric effects are also important for acid sites fixed on a surface; it seems that it is more difficult for methanol molecules to reach the protonated carboxylic group when there is a large alkyl chain blocking access.

In an other hand, this decrease of the reaction yield when increasing the length of FA can't be due to a transport resistance ie limit of diffusion as in the case of zeolite or other microporous materials but most likely due to the long chain of fatty acid (stearic acid) which fold into a specific conformation leading to limited diffusion of the following species of FA.

In order to explain the acidic performance of H–Al–SBA-15 in the esterification of lauric acid with methanol, a reaction mechanism is proposed, involving the role of Brønsted acid sites of the catalyst (Scheme 1). Moreover, ^{1}H-NMR and infrared spectroscopy analytical

Table 4 The effect of acid and alcohol chain length on the esterification reaction over Al–SBA-15–50 catalyst

Acid chain length effect		Alcohol chain length effect	
Acid	Conversion (%)	Alcohol	Conversion (%)
Lauric, C_{12}	90	Methanol C_1, CH_3OH	90
Palmitic, C_{16}	86	Ethanol C_2, CH_3CH_2OH	84
Stearic, C_{18}	83		

Reaction conditions: fatty acid (16 mL), alcohol (1 mmol), Al–SBA-15–50 (5 wt%), 70 °C, 8 h

Scheme 1 Plausible reaction mechanism of the esterification over Al–SBA-15 as a Brønsted acid

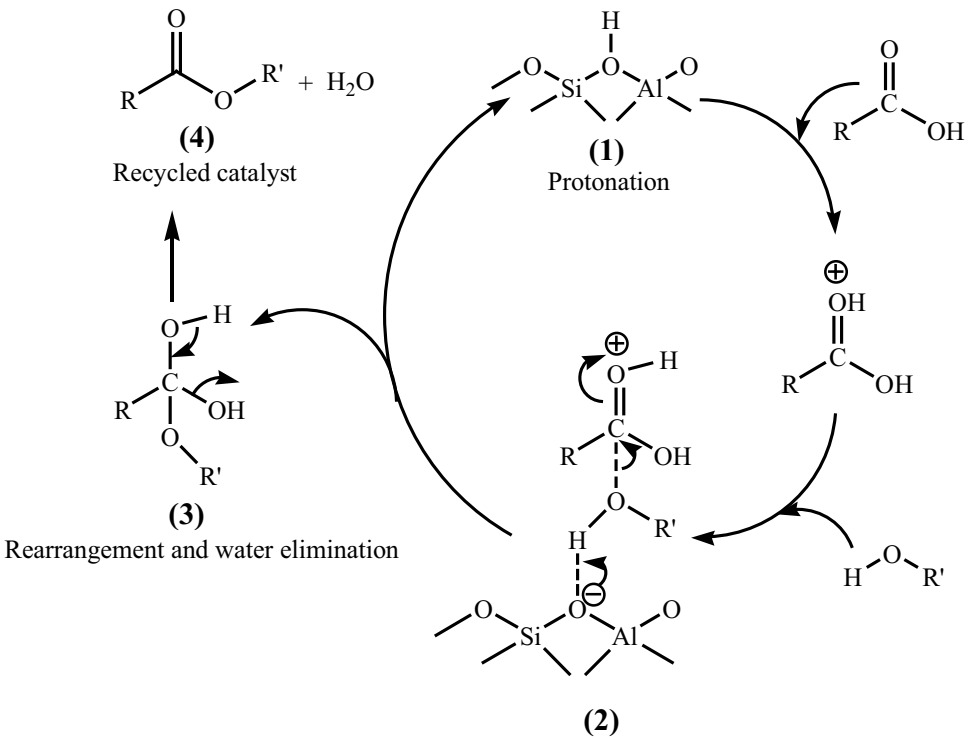

data confirmed that the obtained product (methyl Laurate) is the result of the esterification reaction with the highest yield (90%): ^{1}H-NMR (300 MHz, $CDCl_3$): 0.869 (t, 3H), 1.253 (m, 16H), 1.620 (m, 2H), 2.300 (t, 2H), 3.640 (s, 3H). IR: $\nu_{C-H} = 2884\ cm^{-1}$, $\nu_{CO-O} = 1738\ cm^{-1}$, $\nu_{O-C} = 1193\ cm^{-1}$.

4 Conclusion

Al–SBA-15 supports with three Al_2O_3/SiO_2 ratios (50, 75, and 100), via the present post-synthesis method, have been successfully synthesized.

The structural and textural properties of this catalyst were measured using various analytical instruments. The XRF analysis confirmed the aluminium incorporation. N_2 adsorption and XRD results indicate that well defined hexagonal mesoporous structure are obtained even after alumination process. Furthermore, it seems that aluminium incorporation leads to the decrease of microporosity as it has been showed by N_2 adsorption (DFT). The change in structural and textural parameters compared to siliceous SBA-15 proved the incorporation of aluminium into the framework especially into the wall surface of Al–SBA-15. Moreover, TEM measurements confirmed the best ordered structures. The changes in hydrophobic properties and surface charge show that aluminium is incorporated into the SBA-15 framework and is related to lower silanol groups concentration after Al post synthesis.

The solid catalysts Al–SBA-15 are active in the esterification of lauric acid with methanol at lower reaction temperature. The catalyst conversion of Al–SBA-15 with Si/Al = 100, 75, and 50 were 76, 79, and 85%, respectively.

The correlation between structural/textural properties and the acid activity suggests that the total acidity is caused by the formation of additional surface groups with strong Brønsted acid site. In fact, highly Al ordered mesoporous structure with negative surface charge are obtained. This charge is one of important reason for the increase in the generation of the Brønsted acid sites on the Al–SBA-15 catalysts in the FA esterification.

Moreover, Al–SBA-15–50, which exhibits high Al content, provides the highest catalytic activity even when its structure is slightly affected. However, further studies of the combined effect of other parameters that certainly influence the process have to be considered.

Finally, the obtained results present Al–SBA-15 as an alternative for biodiesel production.

Acknowledgements Z. Talha thanks Dr. Ali-Dahmane Toufik (ESSAT, Tlemcen, Algeria) for valuable assistance in the early and the last stages of this work. The authors are grateful to the reviewers for their constructive comments and corrections that improved the manuscript and also to Dr. Francesco Di Renzo for TEM analysis of Al–SBA-15-50.

References

1. McCusker LB, Liebau F, Engelhardt G (2003) Microporous Mesoporous Mater 58:3–13
2. Fedeyko JM, Vlachos DG, Lobo RF (2006) Microporous Mesoporous Mater 90:102–111
3. Zhao D, Huo Q, Feng J, Chmelka BF, Stucky GD (1998) J Am Chem Soc 120:6024–6036
4. Li Q, Wu Z, Tu B, Park SS, Ha CS, Zhao D (2010) Microporous Mesoporous Mater 135:95–104
5. Zhao D, Feng J, Huo Q, Melosh N, Fredrickson GH, Chmelka BF, Stucky GD (1998) Science 279::548–552
6. Yue YH, Gédéon A, Bonardet JL, d'Espinose JB, Melosh N (2000) Stud Surf Sci Catal 129:209–218
7. Liu H, Wang H, Shen J, Sun Y, Liu Z (2008) Catal Today 131:444–449
8. Ouargli R, Hamacha R, Benharrats N, Boos A, Bengueddach A (2015) J Porous Mater 22:511–520
9. Occelli ML, Biz S, Auroux A, Ray GJ (1998) Microporous Mesoporous Mater 26:193–213
10. Sakthivel A, Dapurkar SE, Gupta NM, Kulshreshtha SK, Selvam P (2003) Microporous Mesoporous Mater 65:177–187
11. Mokaya R, Jones W (1998) Chem Commun 17:1839–1840
12. Mokaya R, Jones W (1999) J Mater Chem 9:555–561
13. Ma J, Qiang LS, Wang JF, Tang XB, Tang DY (2011) J Porous Mater 18:607–614
14. Zeng S, Blanchard J, Breysse M, Shi Y, Shu X, Nie H, Li D (2005) Microporous Mesoporous Mater 85:297–304
15. Hu W, Luo Q, Su Y, Chen L, Yue Y, Ye C, Deng F (2006) Microporous Mesoporous Mater 92:22–30
16. Anderson M, Klinowski XJ (1986) J Chem Soc Faraday Trans 82:1449
17. Inagaki S, Fukushima Y, Kuroda K K (1996) J Colloid Interface Sci 180:623–624
18. Pires J, Pinto M, Estella J, Echeverria JC JC (2008) J Colloid Interface Sci 317:206–213
19. Zhang K, Lively RP, Noel JD, Dose ME, Cool BAM, Chance RR, Koros WJ (2012) Langmuir 28:8664–8673
20. Thommes M, Mitchell S, Perez-Ramirez J (2012) J Phys Chem 116:18816–18823
21. Henninger SK, Schmidt FP, Nunez T, Henning MH (2005) Adsorption 11:361–366
22. Zhao G, Zhao Z, Wu J, Ye D (2014) J Spectroscopy 2014:7 (**Article ID 965037**)
23. Nieto A, Balas F, Colilla M, Manzano M, Vallet-Regí M (2008) Microporous Mesoporous Mater 116:4–13
24. Kokunešoski M, Gulicovski J, Matovic B, Logar M, Milonjic SK, Babic B (2010) Mater Chem Phys 124:1248–1252
25. Mahouche-Chergui S, Grohens Y, Balnois E, Lebeau B, Scudeller Y (2014) Mater Sci Appl 5:953–965
26. Rivoira L, Appendini M, Fiorilli S, Onida B, Del Bubba M, Bruzzoniti MC (2016) Environ Sci Pollut Res 23:21682–21691
27. Yadav GD, Mehta PH (1994) Ind Eng Chem Res 33:2198–2208
28. Altiokka MR, Çitak A (2003) Appl Catal Gen 239:141–148
29. Ayturk E, Hamamci H, Karakas G (2003) Green Chem 5:460–466
30. Marchetti JM, Miguel VU, Errazu AF (2007) Fuel 86:906–910
31. Marchetti JM, Errazu AF (2008) Biomass Bioenerg 32:892–895
32. Mbaraka IK, Radu DR, Lin VS-Y, Shanks BH (2003) J Catal 219:329–336
33. Rabindran Jermy B, Pandurangan A (2005) Appl Catal A Gen 288:25–33
34. Carmo AC, de Souza LKC, da Costa CEF, Longo E, da Rocha Filho GN (2009) Fuel 88:461–468
35. Jiménez-Morales I, Santamaría-González J, Maireles-Torres P, Jiménez-López A (2011) App Catal B Environ 105:199–205
36. Lanzafame P, Temi DM, Perathoner S, Centi G, Macario A, Aloise A, Giordano G (2011) Catal Today 175:435–441
37. Liang C, Wie MC, Tseng HH, Shu EC (2013) J Chem Eng 223:785–794
38. Gonzalez-Arellano C, Arancon RAD, Luque R (2014) Green Chem 16:4985–4993
39. Zhao D, Sun J, Li Q, Stucky GD (2000) Chem Mater 12:275–279
40. Luan Z, Hartmann M, Zhao D, Zhou W, Kevan L (1999) Chem Mater 11:1621–1627
41. Brunauer S, Emmett PH, Teller E (1938) J Am Chem Soc 60:309–319
42. Zhao D, Wan Y, Zhou W (2013) Ordered mesoporous materials, 1st edn. (Wiley-VCH & Co. KGaA., Weinheim)
43. Sing KSW, Everett DH, Haul RAW, Moscou L, Pierotti RA, Rouquérol J, Siemieniewska T (1985) Pure Appl Chem 57:603–619
44. Thommes M, Kaneko K, Neimark AV, Olivier JP, Rodriguez-Reinoso F, Rouquerol J, Sing KSW (2015) Pure Appl Chem 87:1051–1069
45. Samaké D, Thomas F, Greneche JM, Poinsignon C, Pléa M, Debionne J L, Charlet L (2012) J Soc Ouest-Afri Chim A 34:1–11
46. Kao HM, Ting CC, Chao SW (2005) J Mol Catal A Chem 235:200–208
47. Chen S, Li J, Zhang Y, ZhaoY, Liew K, Hong J (2014) Catal Sci Technol 4:1005–1011
48. Li J, Wang L, Qi T, Zhou Y, Liu C (2008) Microporous Mesoporous Mater 110:442–450
49. Kumaran GM, Garg S, Soni K, Kumar M, Gupta JK, Sharma LD, Rama Rao KS, Murali Dhar G (2008) Microporous Mesoporous Mater 114:103–109
50. Brahmi L, Ali-Dahmane T, Hamacha R, Hacini SH (2016) J Mol Catal A Chem 423:31–40
51. Miyazawa K, Inagaki S (2000) Chem Commun 21:2121–2122
52. Galarneau A, Cambon H, Renzo FD, Fajula F (2001) Langmuir 17:8328–8335
53. Esparza JM, Ojeda ML, Campero A, Hernández G, Felipe C, Asomoza M, Cordero S, Kornhauser I, Rojas F (2005) J Mol Catal A Chem 228:97–110
54. Sonwane CG, Ludovice PJ (2005) J Mol Catal A Chem 238:135–137
55. Zhang F, Yan Y, Yang H, Meng Y, Yu C, Tu B, Zhao DY (2005) J Phys Chem B 109:8723–8732
56. Li Q, Wu Z, Tu B, Park S, Ha C, Zhao D (2010) Microporous Mesoporous Mater 135:95–104
57. Yang RT (1987) Gas separation by adsorption processes. Imperial College Press, London
58. Song SW, Hidajat K, Kawi S (2007) Chem Commun 42:4396–4398